

# Simulation of temperature extremes over West Africa and the Eastern Sahel with MPAS

Laouali Ibrahim Tanimoune<sup>1</sup>, Gerhard Smiatek<sup>2</sup>, Harald Kunstmann<sup>2,3</sup>,  
Babatunde J. Abiodun<sup>4</sup>

<sup>1</sup>Department of Meteorology and Climate Science, Federal University of Technology of Akure, Nigeria

<sup>2</sup>Institute of Meteorology and Climate Research (IMK-IFU), Karlsruhe Institute of Technology,

Kreuzteckbahnstr.19, 82467 Garmisch-Partenkirchen, Germany

<sup>3</sup>Institute of Geography, University of Augsburg, Augsburg, Germany

<sup>4</sup>Department of Environmental and Geographical Science, University of Cape Town, Cape Town, South  
Africa

## Key Points:

- Multiple MPAS runs with SST and sea ice extent as the only boundary condition are used to investigate extremes of temperature and heat waves.
- MPAS reveals moderate cold biases for all investigated temperature indices.
- Long term runs as well as short term runs with selected SST years yield similar results.

---

Corresponding author: Gerhard Smiatek, [gerhard.smiatek@kit.edu](mailto:gerhard.smiatek@kit.edu)

## Abstract

A large ensemble of 51 simulations with the Model for Prediction Across Scales (MPAS) has been applied to assess its ability to reproduce extreme temperatures and heat waves in the area of West Africa and the Eastern Sahel. With its global approach the model avoids transition errors influencing the performance of limited area climate models. The MPAS simulations were driven with sea surface temperature (SST) and sea ice extent as the only boundary condition. The results reveal moderate cold biases in the range from  $-0.6^{\circ}$  to  $-0.9^{\circ}$  C for the daily mean temperature and  $-1.4^{\circ}$  to  $-2.0^{\circ}$  C for the area mean of the daily maximum temperature. The bias in the number of tropical nights ranges from +3 to -10 days. An underestimation by up to 50% is also present regarding the number of summer days. The heat wave duration index is underestimated regionally by 10% to 60%. Compared to the reanalyses, the biases revealed by the MPAS simulations are generally smaller than with measured observational reference. The results from long term runs and from short term runs with selected SST years are similar. Shortcomings in the reproduction of the temperature and precipitation indices found in the present investigation indicate that the global MPAS approach does provide a fidelity similar to that of the regional climate models.

## Plain Language Summary

Large number of simulations with the global weather and climate model MPAS has been applied to investigate extreme temperatures and related heat waves. The considered area is West Africa and the Eastern Sahel. In the simulations sea surface temperature and sea ice extent were the only boundary condition. The results reveal moderate underestimation in the range from  $-0.6^{\circ}$  to  $-0.9^{\circ}$  C for the daily mean temperature. The error the area mean of the daily maximum temperature was  $-1.4^{\circ}$  to  $-2.0^{\circ}$  C. An underestimation by up to 50% is also present in the number of summer days. The heat wave duration index is underestimated regionally by 10% to 60%. Obtained results in the reproduction of the observed temperatures and precipitation show that the global MPAS model provides results similar to that of the regional climate models.

## 1 Introduction

West Africa (WA) and the Eastern Sahel are characterized by high temperatures and large variability in rainfall (Nicholson & Webster, 2007; Sultan et al., 2013; Poan

et al., 2016) and have been historically affected by extreme weather anomalies. A long-standing example are the droughts of 1974–1975 over the Sahel. They caused severe increases in mortality in the population and and livestock, and despite the recent occurrence of a greening, the Sahel region is still suffering from these droughts (Janicot et al., 1996; Cook, 2008).

Several studies have provided evidence for a considerable warming in West Africa and the Sahel in the recent past. New et al. (2006) showed that most stations in West Africa reveal positive trends in the minimum and maximum temperature over the period 1961–2000. That study also found increases in both the number of hot days and of cold days. Evaluating reanalyses and CORDEX models, Adeniyi and Oyekola (2017) found that the magnitude of the frequencies of heat waves in West Africa has increased. Oueslati et al. (2017) found that heat waves are spatially increasing with high intensity. Similar findings are reported concerning increases in temperatures and the frequencies of heat waves, particularly in the Sahel (Ringard et al., 2016; Russo et al., 2016; Dosio, 2017). Further increases are projected for the future. From results based on CMIP5 model simulations, Ringard et al. (2016) reported significant increases in heat waves for the Sahel in all applied scenarios.

An increase in the severity and frequency of heat wave events can lead to the loss of human lives and the destruction of crops. Extreme temperatures and heat waves strongly affect the socio-economic conditions in various sectors, such as agriculture, infrastructure, and energy (Lobell et al., 2011; Coumou & Rahmstorf, 2012; Perkins et al., 2015). A weak economy, an inefficient policy, and a limited resilience increase the vulnerability. Hence, modeling tools capable of simulating extreme present and expected future climate conditions have gained increasing importance for the support of policymakers.

The scientific aim of this study is the evaluation of the global Model for Prediction Across Scales (MPAS), driven with sea surface temperature (SST) and sea ice extent as the only boundary condition, with regard to its ability to simulate extreme temperatures and heat waves in West Africa and the Eastern Sahel. In addition, basic precipitation indices are investigated. With its global approach, the model prevents the errors commonly introduced in regional climate models (RCMs) in the transition zone from the driving GCM (General Circulation Model) to the regional model, and thus provides an additional tool applicable to the vital questions related to present and future climate

conditions. Dosio et al. (2022) points out that RCMs do not improve the simulation ability of large-scale fields compared to GCMs.

So far, MPAS has only been applied to this region by Heinzeller et al. (2016), who had a focus on the reproduction of the dynamics of the West African monsoon (WAM) and the associated precipitation. Unlike RCM applications, global MPAS runs are not confined by a driving model but, besides the boundary conditions, depend on their initialization. Thus, an additional aim of this study is the comparison of two different initialization procedures.

This study considers the summer season as the most important period for the regional economy, which greatly relies on agriculture, which depends on the seasonal rainfall and the behavior of the monsoon rains (Sivakumar et al., 2014) and is generally practiced during the summer. Any changes during this crucial period often have a devastating effect on socio-economic activities and food security in the region (Dilley & Heyman, 1995; Haile, 2005; Omotosho & Abiodun, 2007). Drought, excessive rains, or heatwaves during the growing season can potentially diminish crop yield, especially in the Sahel, where water is a particularly determining element for the growth of the crops (Ahmed et al., 2015).

The present study is structured as follows: Section 2 describes the applied model, reference data, investigation areas and the evaluation indices. The results of the evaluation are presented and discussed in Section 3, and conclusions are drawn in Section 4.

## 2 Material and methods

### 2.1 MPAS model

The applied meteorological model is the Model for Prediction Across Scales (MPAS), which is based on unstructured Voronoi meshes and C-grid discretization (Thuburn et al., 2009; Ringler et al., 2010). MPAS-atmosphere (Skamarock et al., 2012), used in the present study, is a global, fully compressible non-hydrostatic model (Klemp, 2011). The model is run at an approximately 60-km resolution mesh with a total of 163,842 cells, applying the mesoscale reference physics suite, 55 vertical levels up to a height of 30 km, and 4 soil levels. The land-surface physics component is the Community Noah Land Surface Model (Noah-LSM) (Chen et al., 1996).

Table 1 shows the associated parametrization schemes of the standard model configuration. The RRTMG (Clough et al., 2005) long-wave and short-wave radiation scheme uses a fixed value for carbon dioxide, reflecting the conditions of the years around 2004. The static input fields applied are the MODIS 20-class land cover based on global land cover climatology collected in 2001–2010 at 500-m resolution (Broxton et al., 2014) and the Global Multi-Resolution Terrain Elevation Data (GMTED2010) (Danielson & Gesch, 2011) topography. The surface albedo and vegetation fraction are updated monthly from MODIS climatology.

**Table 1.** Parametrization schemes used by the simulations

Parametrization	Scheme
Convection	New Tiedtke
Microphysics	WSM6
Land surface	Noah-LSM
Boundary layer	YSU
Surface layer	Monin–Obukhov
Radiation, LW	RRTMG
Radiation, SW	RRTMG
Cloud fraction for radiation	Xu–Randall
Gravity wave drag by orography	YSU

## 2.2 Performed simulations

An MPAS simulation with SST and sea ice extent as the only boundary condition does not reproduce the weather of a specific year, but it creates weather patterns that fit these conditions. Thus, in order to reproduce the observed climatology, multiple runs with different initialization dates are required. The present article presents 51 MPAS simulations. They form three experiments, denoted by MPAS\_A, MPAS\_B and MPAS. Experiment MPAS\_A applies the initialization data, SST and sea ice extent from the ERA-Interim reanalysis (Dee et al., 2011) and follows the procedure applied by Smiatek and Kunstmann (2023). Six years have been selected according to the SST anomaly in the Gulf of Guinea during the summer season (Figure 2). The Gulf of Guinea has a central

influence on the precipitation in West Africa (Son & Seo, 2020). The considered period covers 30 years around 2004, from 1990 to 2019. Specific years are 1992 and 1997, revealing a positive anomaly, 1998 and 2010 with a negative anomaly, and 2003 and 2016 are neutral. These anomalies basically correspond to positive and negative ENSO states. Within each SST-year, five simulations initialized from May 15 through May 19 and run until September 1 have been performed.

Experiment MPAS\_B is a continuous MPAS simulation initialized in December 1980, from which the results for the period 1990–2010 are applied in the present investigation. For the initialization, the SST and sea ice extent data from the Climate Forecast System Reanalysis (CFSR) (Saha et al., 2014) are used. CFSR data is available until 2010. The chosen period covers the largest SST anomalies in the Gulf of Guinea (Figure 2).

The MPAS experiment consists of MPAS\_A and MPAS\_B simulations lumped into a single ensemble. The investigated period is the summer season (JJA).

### 2.3 Observational reference and investigated areas

The present investigation uses a set of available gridded temperature and precipitation reference data at monthly and daily resolution. These are interpolated station and gauge measurements (CPC, CRU), extended satellite measurements (CHIRTS), as well as state of the art reanalyses (ERA5, JRA-55, MERRA-2, NCEP-2). Table 2 provides some details about the applied data. With the exception of the CHIRTS data, which is available only up to 2016, all data sets cover the investigated period, 1990–2019. CRU only provides monthly resolution and therefore is used only in the basic statistics.

The results of the performed simulations are analyzed in two areas in the Sahel region, SAH\_W and SAH\_E, and one area at the coast of Guinea, GUI\_C, as well as for the entire region. There are no standard evaluation areas available so far for West Africa and the Sahel. However, the areas SAH\_W and SAH\_E have been used by several studies (Dosio et al., 2021a, 2021b; Smiatek & Kunstmann, 2023), and thus allow putting the results in the context of previous investigations. Figure 1 shows the MPAS 60-km mesh and the investigation areas.

**Table 2.** Reference data applied in the present study. G denotes the gauge, M, the monitoring station, R, reanalysis, and S, satellite measurements

Acronym	Name	Resolution	Type	Reference
ERA5	ECMWF ERA5	0.25°	R	Hersbach et al. (2020)
JRA-55	Japanese 55-year Reanalysis	1.25°	R	Kobayashi and Iwasaki (2016)
MERRA-2	Modern-Era Retrospective Analysis for Research and Application, v. 2	0.5 x 0.625°	R	Gelaro et al. (2017)
NCEP-2	NCEP-DOE Reanalysis 2	1.875°	R	Kanamitsu et al. (2002)
CHIRTS	Climate Hazard Group Infrared Temperature with Station Data	0.25°	M,S,R	Funk et al. (2019)
CPC	Unified Gauge-Based Analysis of Global Daily Precipitation	0.5°	G	Xie et al. (2007)
CRU	Climate Research Unit	0.5°	G,M	Harris et al. (2020)

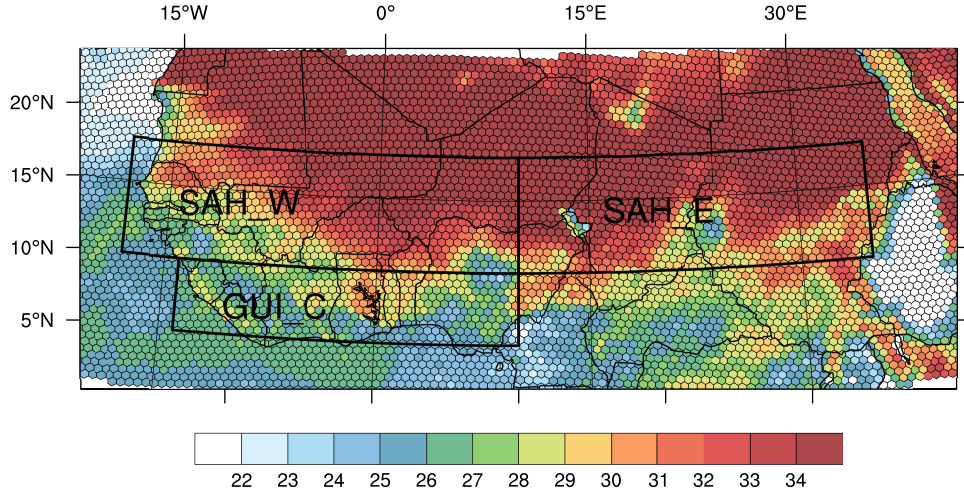


**Figure 1.** MPAS 60 mesh and investigated areas SAH\_W, SAH\_E and GUI\_C. Simulated 2-m temperature 01.07.2010:12:00 UTC)

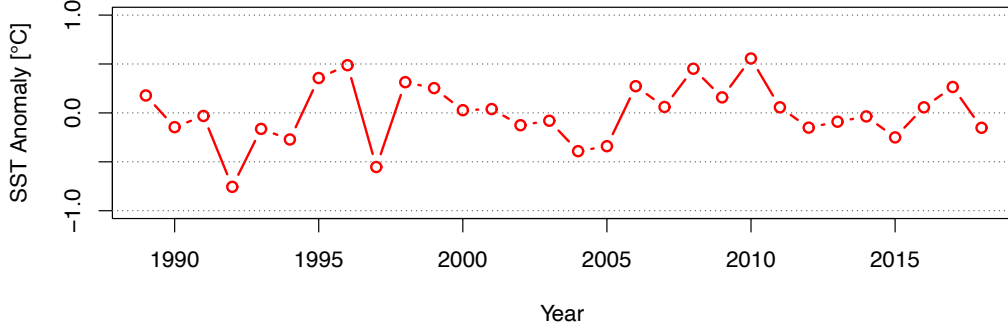


**Figure 2.** SST anomaly over the Gulf of Guinea as in ERA-Interim 1989–2018

## 2.4 Investigated indices

The investigated temperature related indices were selected from the perspective of the socio-economic activities in the investigated region and comprise indices used by similar investigations (Engdaw et al., 2022), mostly defined by the Expert Team on Climate Change Detection, Monitoring and Indices (ETCCDI)(Karl et al., 1999) with adjusted thresholds. They are the daily mean (TG), minimum (TN) and maximum (TX) temperature, the number of tropical nights (TR) with  $TN > 24^\circ$ , the percentage of warm nights (TN90p) with  $TN > 90$ th percentile, the number of summer days (SU) with  $TX > 35^\circ$ , the percentage of warm days (TX90p) with  $TX > 90$ th percentile, and the heat wave duration index (HWDI) with  $TX > TX_{norm} + 3^\circ$  over at least three days.  $TX_{norm}$  is calculated as the mean of the maximum temperatures of a five-day window over all simulations and with the reference data from the entire investigated period.

The indices related to precipitation are the daily mean precipitation (RR), the number of wet days (RR1), and the maximal daily rainfall (RX1day). These indices allow a comparison with the investigation of the observed and simulated precipitation characteristics provided by Dosio et al. (2021a) and Dosio et al. (2021b).

Table 3 shows the indices, their definitions, and their units. All indices are calculated for land points only and were derived from instantaneous 3-hourly MPAS output.

## 3 Results

Figure 3 shows the distributions of the area mean summer (JJA) mean temperature TG in the investigated areas SAH.W, SAH.E and GULC for both the reference data

**Table 3.** List of indices analyzed in this study. The indices are calculated on a seasonal (JJA) basis.

Index	Definition	Units
TG	Seasonal mean of daily mean temperature	°C
TN	Seasonal mean of daily minimum temperature	°C
TX	Seasonal mean of daily maximum temperature	°C
TXx	Seasonal maximum of TX	°C
TR	Number of tropical nights with $TN > 24^{\circ}$	d
TN90p	Percentage of days when $TN > 90$ th percentile	%
SU	Number of summer days with $TX > 35^{\circ}$	d
TX90p	Percentage of days when $TX > 90$ th percentile	%
HWDI	Heat wave duration index. $TX > TX_{norm} + 3^{\circ}$ over at least 3 days	d
RR	Daily mean precipitation	mm/d
RR1	Number of wet days when $RR \geq 1$ mm	d
RX1day	Maximal daily RR	mm/d

and the MPAS simulations. It reveals that the results obtained from MPAS are well within range, and there are only small differences between the different simulation approaches of MPAS\_A and MPAS\_B.

Concerning the ranges and the area mean value, there are substantial differences in the reference data (Table 4). In the SAH\_W area, the mean value TG in the reanalyses extends from  $28.4^{\circ}\text{C}$  to  $29.4^{\circ}\text{C}$ , the range in the data based on observations is from  $29.5^{\circ}\text{C}$  to  $29.9^{\circ}\text{C}$ . MPAS shows, with  $28.7^{\circ}\text{C}$ , a cold bias of  $-0.6^{\circ}\text{C}$  in relation to the mean of the entirety of the reference data, of  $-0.4^{\circ}\text{C}$  in relation to the mean value of the reanalysis products, and  $-1.1^{\circ}\text{C}$  to the observational reference. The corresponding biases in the SAH\_W area are  $-0.6^{\circ}$ ,  $-0.3^{\circ}$ ,  $-1.2^{\circ}\text{C}$ , and in the GUL\_C area,  $-0.9^{\circ}$ ,  $-0.5^{\circ}$  and  $-1.6^{\circ}\text{C}$ .

These results are comparable to the findings from previous simulation experiments. For instance, Hernández-Díaz et al. (2013) found, over West Africa, biases in the simulations with the Canadian Regional Climate Model (CRCM5) in the range from  $-2^{\circ}\text{C}$  to  $2^{\circ}\text{C}$ . Gbobaniyi et al. (2014) found, with the WRF model, biases of  $0.8^{\circ}\text{C}$  over West Africa, of  $0.8^{\circ}\text{C}$  over Guinea, and  $1.6^{\circ}\text{C}$  over the Sahel during the JAS (July, August, September) period. With the RCA4 model, Nikiema et al. (2017) reported biases of  $1.2^{\circ}\text{C}$  over WA,  $1^{\circ}\text{C}$  over Guinea and  $1.2^{\circ}\text{C}$  over the Sahel. Kim et al. (2014) concluded from the CORDEX-Africa experiment with 10 regional climate models, seasonal (JJAS) biases ranging from  $-0.5^{\circ}\text{C}$  to  $0.8^{\circ}\text{C}$  over West Africa. Dosio et al. (2015) found in simulations with the COSMO-CLM model cold biases up to  $3^{\circ}\text{C}$  in the Guinea region and the southern Sahel. Careto et al. (2018) reported in CORDEX-Africa experiments cold biases in most of Africa for all RCMs, with the largest biases over the Sahel. With the MPAS model, Maoyi and Abiodun (2021) found a cold bias up to  $2^{\circ}\text{C}$  over the Indian Ocean and cold biases up to  $1.2^{\circ}\text{C}$  within the southern African countries. They attributed the error primarily to the coarser resolution of 240 km applied in the simulations.

Figures 4 to 5 depict boxplots of the mean daily maximum temperatures TX and TXx, for the reference data and the MPAS simulations. The corresponding area mean values are shown in Table 4. Compared to the mean values, the cold biases are larger. In the SAH\_W area, a cold bias of  $-1.4^{\circ}\text{C}$  compared to the mean of all the reference data is present for TX. It is  $-2.2^{\circ}\text{C}$  for TXx. The cold biases related to the reanalyses are smaller. However, it has been taken into account that NCEP-2 has a much lower resolu-

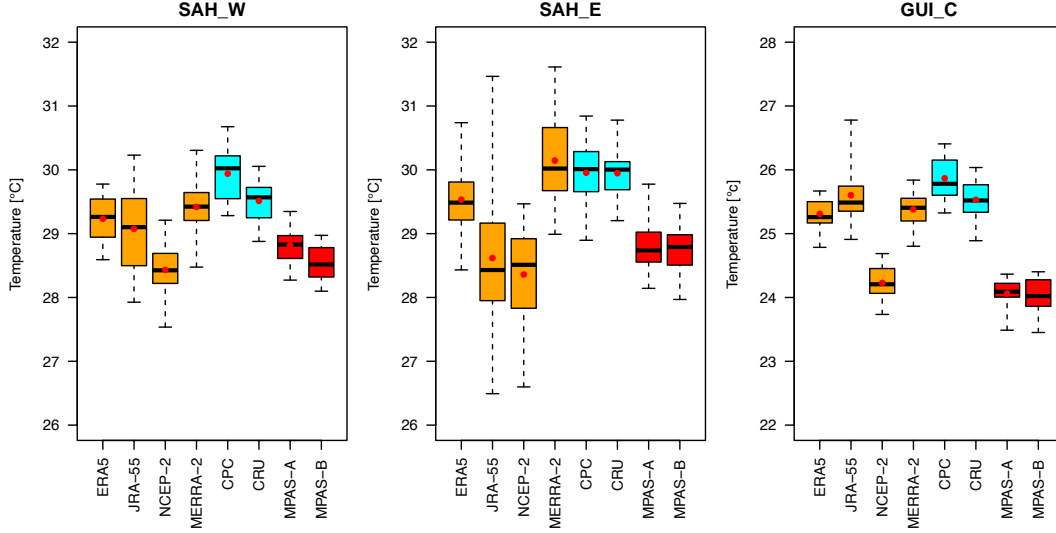


**Figure 3.** Boxplots of the area mean summer (JJA) mean temperature TG in the investigated areas SAH\_W, SAH\_E and GUI\_C

tion. Related to the observations, the MPAS cold biases are larger, at  $-2.1^{\circ}\text{C}$  and  $-2.5^{\circ}\text{C}$ , respectively. The results obtained for the SAH\_E and GUI\_C areas are similar. However, the biases are larger when only the observational reference is considered.

The estimated number of tropical nights is, in SAH\_W and SAH\_E, within the range of the reference data (Figure 6) and only in the GUI\_C area is TR, with 10 days larger, underestimated. When compared to observations only, biases ranging from  $-12$  to  $-20$  days are present. This is about 10% to 80%. The same findings apply to the number of summer days SU (Figure 7), where this number is slightly underestimated, by five days (14%) in the area SAH\_W and by 15 days (33%) in SAH\_E. The number of summer days in the GUI\_C area is very small and therefore not considered here.

Biases in the percentiles TN90p and TX90 reach values of  $-33\%$  and  $-53\%$  in SAH\_W,  $-19\%$  and  $-7\%$  in SAH\_E and  $+7\%$  and  $-46\%$  in GUI\_C when compared to the mean values of the reference data. The biases are larger in SAH\_E and GUI\_C and smaller in SAH\_W when the reference are observations only. Finally, the largest biases, reaching  $-66\%$  in SAH\_W and  $-86\%$  in GUI\_C, are found for the heat wave duration index HWDI. In SAH\_E, this bias is, at 10%, rather small.

In summary, it can be concluded that there are moderate to partly large biases in the summer area mean values of the investigated indices. These are in general cold bi-

**Table 4.** Mean values of temperature indices over the investigation areas for the JJA season, both observed and simulated

Area	Data	TG [°C]	TX [°C]	TXx [°C]	TR [d]	SU [d]	TN90p [%]	TX90p [%]	HWDI [d]
SAH_W	ERA5	29.2	34.3	40.3	51.7	41.1	14.2	20.1	10.7
	JRA-55	29.1	33.2	40.5	52.5	31.1	29.9	34.3	40.9
	NCEP-2	28.4	32.4	40.5	50.2	29.8	5.3	57.5	34.4
	MERRA-2	29.4	34.7	41.3	49.0	41.9	15.1	20.2	18.5
	CPC	29.9	34.5	41.2	58.7	40.7	15.5	15.6	18.6
	CRU	29.5	35.0	-	-	-	-	-	-
	CHIRTS	-	34.9	40.9	68.6	42.5	17.6	17.6	5.5
	MPAS_A	28.8	32.7	38.5	52.3	33.6	13.8	11.5	8.5
	MPAS_B	28.5	32.7	38.6	49.5	31.7	8.1	14.7	6.3
	MPAS	28.7	32.7	38.6	50.9	32.7	11.0	13.1	7.4
SAH_E	ERA5	29.5	34.9	40.4	46.4	49.0	21.0	27.3	14.3
	JRA-55	28.6	32.9	39.4	39.4	34.8	46.9	54.1	40.6
	NCEP-2	28.4	32.7	40.7	41.3	33.9	17.2	76.4	55.1
	MERRA-2	30.1	36.0	41.6	48.2	54.7	26.7	32.5	23.5
	CPC	30.0	35.3	42.0	52.8	47.7	26.9	20.7	24.9
	CRU	29.9	36.4	-	-	-	-	-	-
	CHIRTS	-	37.1	42.6	78.5	61.5	28.7	28.7	8.6
	MPAS_A	28.8	33.2	38.7	51.8	33.6	25.2	22.1	18.1
	MPAS_B	28.8	32.8	38.2	56.4	29.7	19.8	21.7	10.1
	MPAS	28.8	33.0	38.5	54.1	31.7	22.5	21.9	14.1
GULC	ERA5	23.3	28.5	31.9	5.8	0.2	8.4	15.0	0.4
	JRA-55	25.6	28.5	32.3	14.7	1.9	13.1	18.0	9.7
	NCEP-2	24.2	25.9	32.1	8.1	0.1	4.2	55.1	9.1
	MERRA-2	25.4	28.7	32.3	5.0	0.8	9.2	19.7	8.3
	CPC	25.9	29.0	33.4	19.2	0.2	15.6	19.3	7.7
	CRU	25.5	29.2	-	-	-	-	-	-
	CHIRTS	-	29.7	33.4	26.0	0.2	15.6	15.6	0.2
	MPAS_A	24.1	27.4	30.6	3.1	0.0	12.2	15.5	1.1
	MPAS_B	24.1	26.8	30.1	2.0	0.0	11.4	10.3	0.5
	MPAS	24.1	27.1	30.4	2.6	0.0	11.8	12.9	0.8

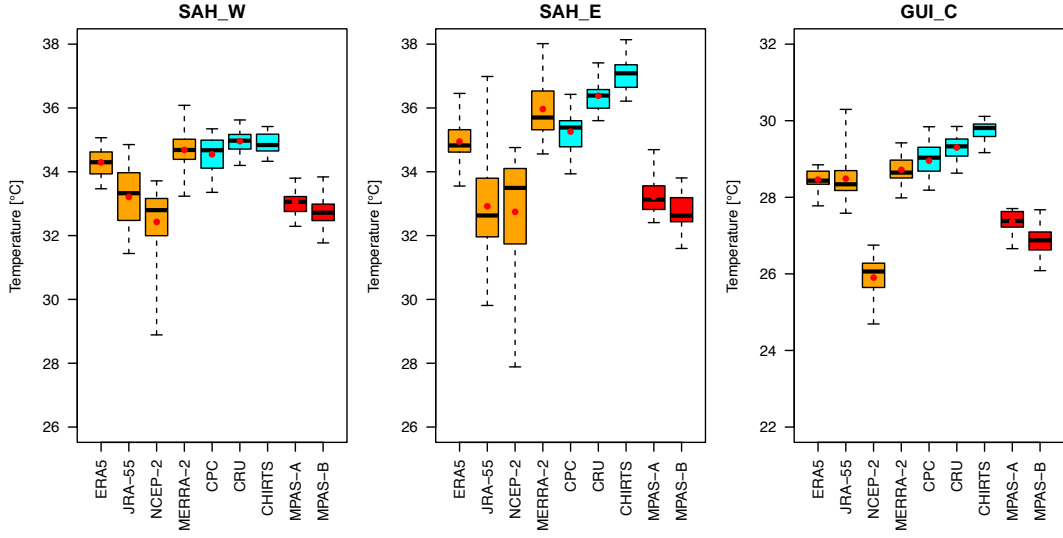


**Figure 4.** Boxplots of mean daily maximum temperature TX for the reference data and MPAS simulation in the investigation areas SAH\_W, SAH\_E and GUI\_C and the summer season (JJA)

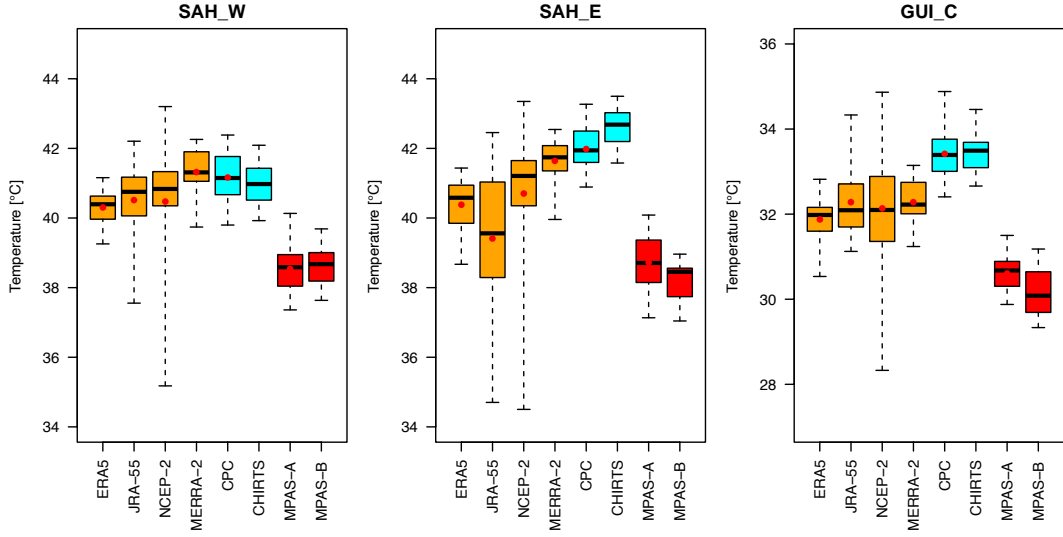


**Figure 5.** Boxplots of maximum daily maximum temperature TXx for the reference data and MPAS simulation in the investigation areas SAH\_W, SAH\_E and GUI\_C and the summer season (JJA)

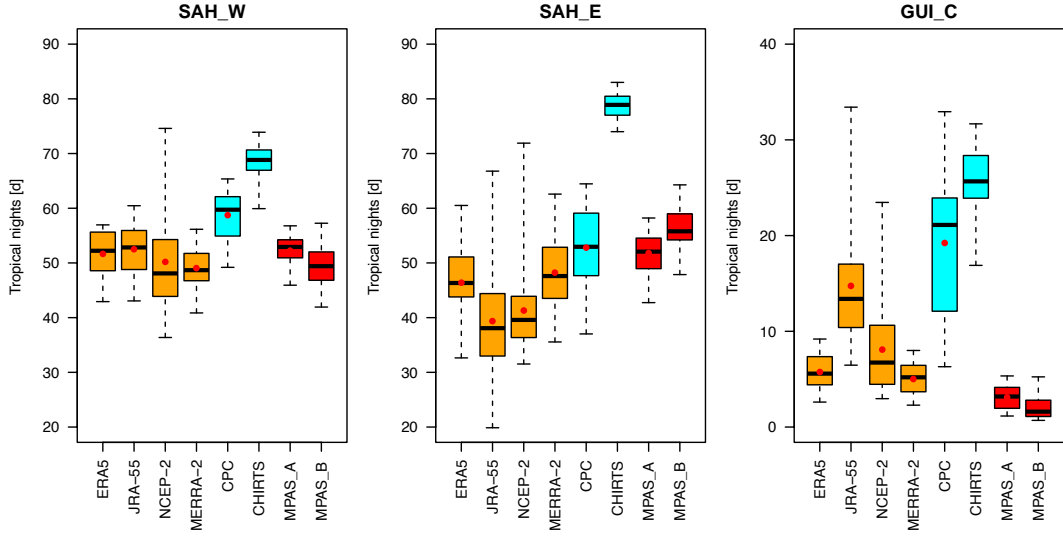


**Figure 6.** Boxplots of the number of tropical nights TR with daily minimum temperature over  $24^{\circ}\text{C}$  for the reference data and MPAS simulations in the investigation areas SAH\_W, SAH\_E and GUI\_C and the summer season (JJA)

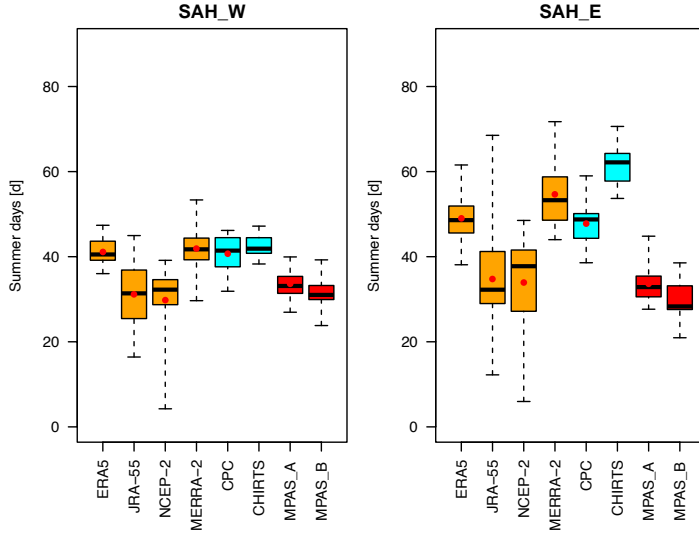


**Figure 7.** Boxplots of the number of summer days SU with temperature over  $35^{\circ}\text{C}$  for the reference data and MPAS simulations in the investigation areas SAH\_W, SAH\_E and GUI\_C and the summer season (JJA)

ases and underestimations of the reference data. The biases are larger when only the observational reference is considered. On the other hand, the ranges in the MPAS simulations and in the observations are similar. Lower biases are found in comparison to the reanalyses, which on the other hand reveal much higher ranges. MPAS reaches, when biases in percent of the reference are considered, the lowest biases in the SAH\_W area in five of the investigated indices. Limiting this comparison to the reference from observations yields the lowest biases in four indices in MPAS\_E and four in MPAS\_W. In the complex coastal area GUI\_C, MPAS simulations reveal the highest biases. As in the CORDEX-experiments (Kim et al., 2014), the biases simulated for West Africa are generally smaller than for the eastern part of the Sahel. This might however be related to the lower density of monitoring stations in this region (Masunaga et al., 2019). Dosio (2017) found, regarding the summer mean temperature (TG), large discrepancies between the individual simulations, with the model spread ranging from 3.5°C over the coast of Guinea, to 7°C, over SAH\_E.

Despite the deficiencies, the general applicability of MPAS to climate simulations can be concluded here. Also, the results obtained from the two procedures employed for initializing the model, MPAS\_A and MPAS\_B, are very similar (Table 4) and demonstrate the equivalence of these approaches to initialization.

Larger biases are found at regional scales. Figure 8 shows maps of the MPAS simulated mean maximum temperature (TX) and differences between MPAS, the mean values of the MPAS\_A and MPAS\_B experiments, and the mean of the applied reference data. In comparison, MPAS reveals a notable cold bias throughout the considered region. Only in the Volta region and in the Western Sahara are there small positive biases. In comparison with the reanalyses, the biases are generally smaller, reveal however, similar negative values with MERRA-2 and CHIRTS. The results with JRA-55 and NCEP-2 differ and show also positive biases. The smallest differences occur with the ERA5 reference. Taking into account the biases in the observations resulting from the rather low station density in some areas and the coarser resolution of the other reanalysis data, it can be concluded that the MPAS performs reasonably well.

The patterns of the differences in the number of summer days (SU) with daily maximum temperature  $TX > 35^\circ \text{C}$  (Figure 9) are similar in the Sahel, showing large underestimations, especially in the eastern part. Positive biases are found in the hot north-

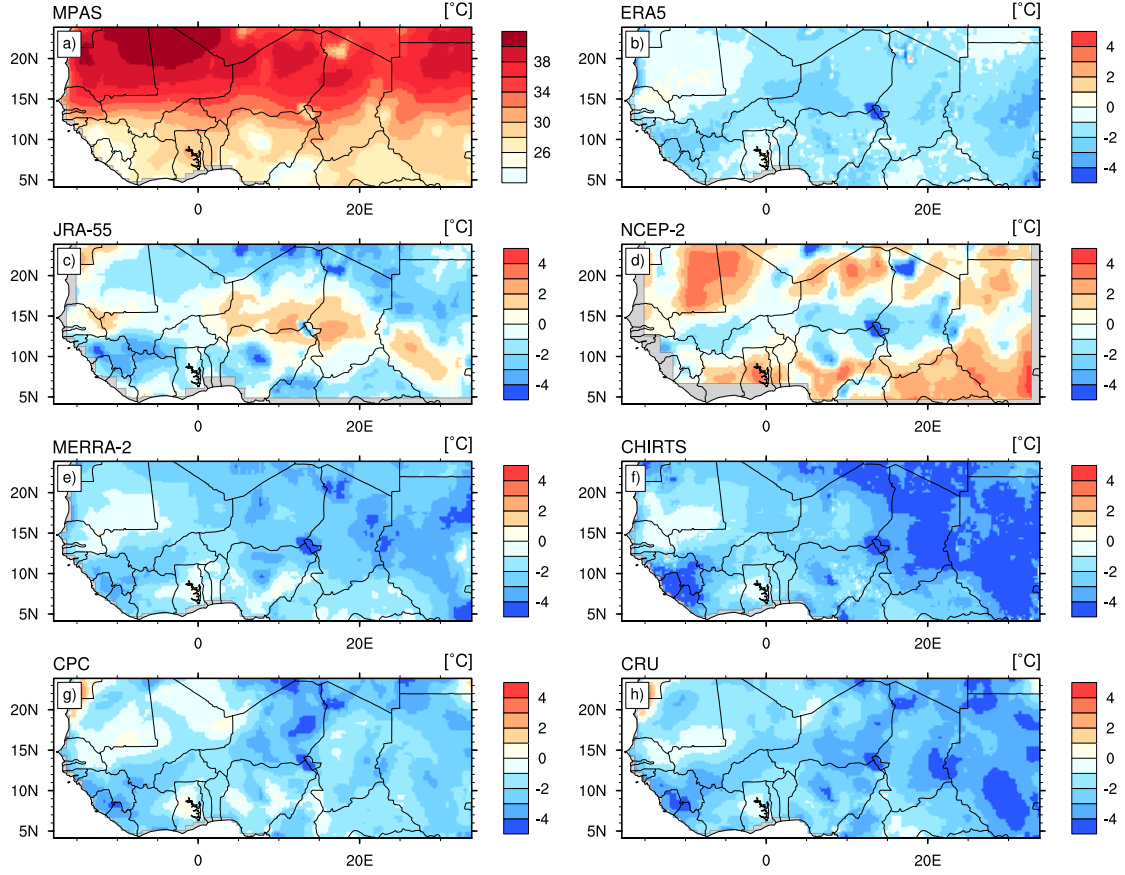


**Figure 8.** Simulated MPAS mean maximum temperature TX and differences between the MPAS and reference data. For the explanation of the acronyms of the reference data, see Table 2.

ern part of the Sahel and Saharan zones, while in WA the biases are rather small. Dosio (2016) argued from the results of the CORDEX-Europe experiment that the underestimation of the number of summer days SU is the consequence of the underestimation of the daily maximum temperature TX. The biases in the southern parts of the investigated area are smaller. However, the number of observed SU days is small there.

The simulated heat wave duration index (HWDI) and the differences between the MPAS and the reference data are shown in Figure 10. The picture here is, however, not clear. While a positive bias dominates in the CHIRTS data, this bias is negative for the CPC observations. The differences from JRA-55 and NCEP-2 are mostly negative. With

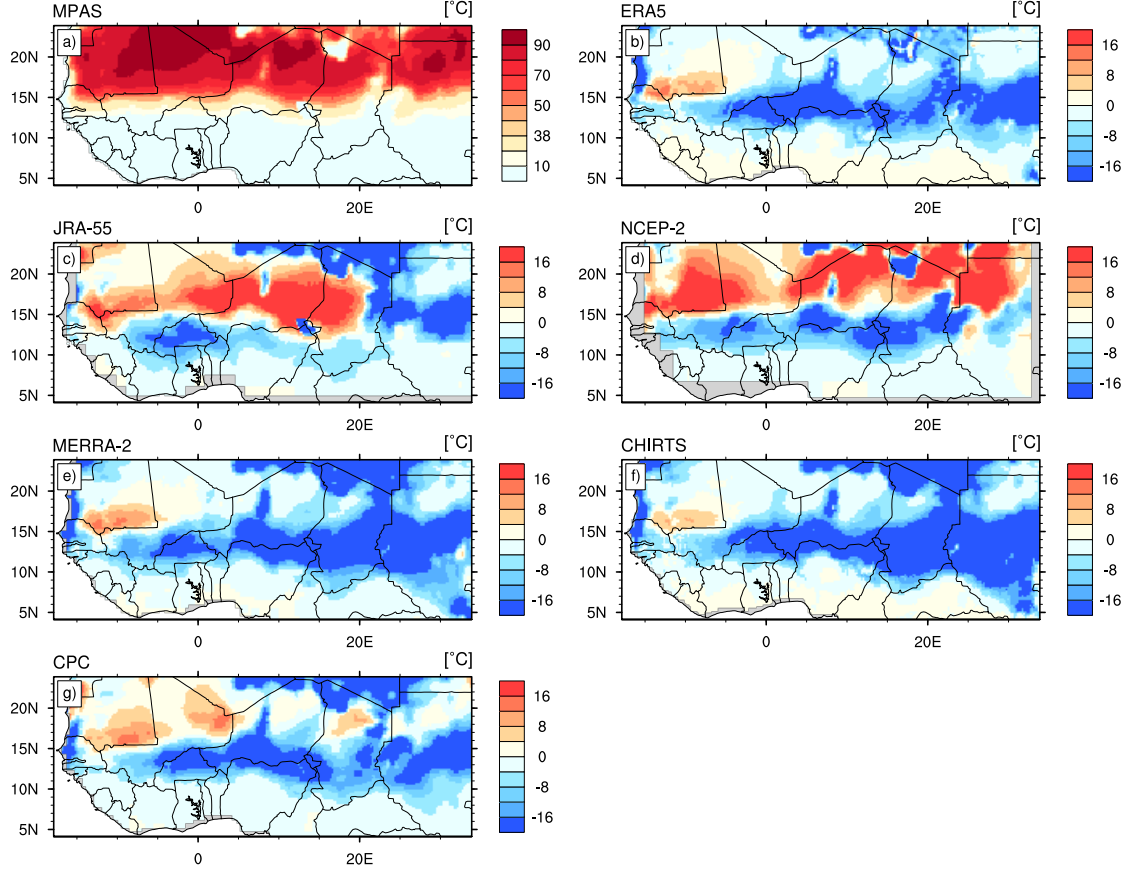


**Figure 9.** As in Figure 8 but for the number of summer days SU with daily maximum temperature  $TX > 35^\circ$

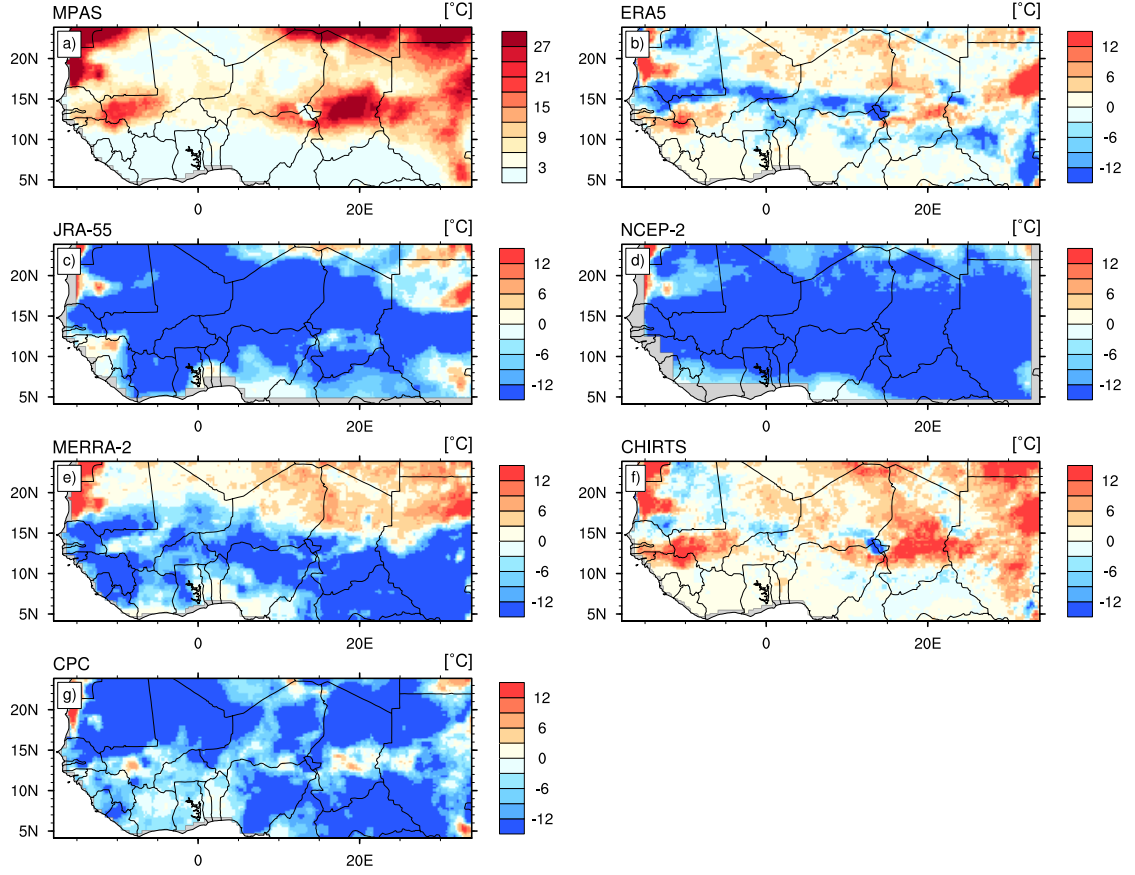


**Figure 10.** As in Figure 8 but for the heat wave duration index HWDI

ERA5 and MERRA-2, positive biases dominate the northern part. In the southern part, the biases are rather negative and larger with the JRA-55 reanalysis. The largest discrepancies seem to occur around the latitude of 15°N.

Summarizing the regional findings, it can be concluded that a cold bias in the TX is evident. It dominates the results obtained for the related temperature indices. Due to large differences between the single reference data, those results are less clear.

The cold biases in MPAS may contribute to dry biases in the simulated rainfall, as the temperature gradient is the origin of jets which in turn transport moisture and the development of rainfall over the Sahel (Grist & Nicholson, 2001). In addition, the deficiencies in precipitation may also be related to the fact that the MPAS underesti-

**Table 5.** Mean values of precipitation indices over the investigation areas for the JJA season, both observed and simulated. S, G and R denote minimum, mean and maximum values of observational datasets for satellite (S), gauge (G) and reanalysis (R) products as presented by Dosio et al. (2021b)

Area	Data	RR mm/d	RR1	RX1day
SAH_W	S	3.7–4.6–7.0	32.8–39.3–47.6	22.0–41.3–68.1
	G	3.9–4.3–4.6	33.8–40.3–49.6	29.1–39.3–46.2
	R	2.8–4.1–5.2	23.8–47.2–63.6	25.7–33.5–43.1
	MPAS_A	2.7	41.5	23.6
	MPAS_B	2.7	41.5	21.2
	MPAS	2.7	41.5	22.4
SAH_E	S	2.1–2.9–4.7	22.1–29.5–37.5	18.2–29.8–51.5
	G	2.5–2.8–3.1	25.9–31.2–38.8	23.3–31.0–40.5
	R	2.4–3.1–3.7	25.9–41.5–49.1	16.7–28.1–44.1
	MPAS_A	2.9	40.3	21.4
	MPAS_B	3.2	50.9	19.7
	MPAS	3.1	45.6	20.6

279 mates the number of summer days. SU can affect the convection and regional precip-  
 280 itation recycling (Arnault et al., 2016) over WA and the Sahel. Nicholson and Webster  
 281 (2007) argued that the reduction in the number of mesoscale convective systems nega-  
 282 tively influences the formation of rainfall over the Sahel.

283 Table 5 shows the results for the investigated precipitation indices in the investi-  
 284 gation areas SAH\_W and SAH\_E in comparisson with observational reference from satel-  
 285 lite, gauge and reanalysis products as presented by Dosio et al. (2021b). It reveals an  
 286 underestimation of the observed amount of daily precipitation RR in the SAH\_W area  
 287 by 1.6 mm/d or 38%, and is outside the range of the observational datasets. In SAH\_E,  
 288 MPAS slightly overestimates the observations, by 4%, and is well within the range of the  
 289 reference data. Only small biases are present in the number of rainy wet days (RR1) with  
 290 precipitation of at least 1 mm in the area SAH\_W. The shortcoming here is the low pre-  
 291 cipitation intensity on wet days. Also, an underestimation on the order of 40% is present  
 292 for the area mean maximum daily rain Rx1day. In SAH\_E, RR1 is overestimated by 37%  
 293 and the maximum daily rain is underestimated by 31%. The investigations of Dosio et  
 294 al. (2021a) based on CMIP5, CIMIP6 global models and CORDEX experiments found  
 295 a large spread between the models. The MPAS results are within the range of those find-  
 296 ings. However, it has to be concluded that it has a significant dry bias for West Africa.

297 Various reasons have been discussed explaining the obvious deficiencies of the cli-  
 298 mate models in reproducing observed temperature and precipitation characteristics in  
 299 WA and the Sahel. They are related to a misplacement of the centre of the monsoon and  
 300 the underestimation of its intensity and to the northern shift of the West African Heat  
 301 Low (Panitz et al., 2014), errors in the simulation of the lateral terrestrial water flow and  
 302 its contribution to land surface evaporation(Arnault et al., 2021), as well as underesti-  
 303 mation of the surface short-wave radiation and latent heat flux, cloudiness, surface wa-  
 304 ter and the surface albedo (Sylla et al., 2009; Diallo et al., 2017; Dieng et al., 2017). In  
 305 applications of the WRF model together with the Noah-LSM, Glotfelty et al. (2021) iden-  
 306 tified the satellite derived albedo climatology as a source of additional errors. Careto et  
 307 al. (2018) linked higher temperatures to evaporative stress and strong soil moisture tem-  
 308 perature coupling in some areas. For the Sahel, however, they stated that precipitation  
 309 regimes are more important. Finally, as pointed out by Heinzeller et al. (2018), the choice  
 310 of physical parametrizations can greatly influence the model’s capabilities, especially the  
 311 accuracy of the surface temperature and precipitation.

In summary, it can be stated that the MPAS global static 60-km mesh approach does not provide higher fidelity than the regional climate models. However, the ability of MPAS to apply variable meshes in a regional refinement and to run in convection permitting mode opens possibilities for improvements, as shown by Heinzeller et al. (2016).

## 4 Conclusions

A large ensemble of 51 simulations with the Model for Prediction Across Scales (MPAS) has been used to assess its ability to reproduce the summer (JJA) extreme temperature and heat waves in the area of West Africa and the Eastern Sahel. With its global approach, the model avoids transition errors influencing the performance of limited area climate models. Also, the simulations are not confined by a driving model. The MPAS simulations were driven by the SST and sea ice extent as the only boundary conditions.

The results reveal moderate cold biases in the range from  $-0.6^{\circ}$  to  $-0.9^{\circ}$  C for the daily mean temperature and increase to  $-1.4^{\circ}$ – $-2.0^{\circ}$  C for the area mean of the daily maximum temperature TX and to  $-2.2^{\circ}$ – $-2.7^{\circ}$  C for TXx as the maximum of TX. The bias in the number of tropical nights TN ranges from +3 to  $-10$  days. An underestimation by up to 50% is also present in the number of summer days SU with TX  $> 35^{\circ}$ C. The percentage of days when TN  $>$  the 90th percentile TN90p as well as the percentage of days when TX  $>$  the 90th percentile TX90p reveal underestimations by up to 50%, and the heat wave duration index HWDI is underestimated by 10%–60%. Compared to the reanalyses, the biases revealed by the MPAS simulations are generally smaller than with the measured observational reference. Because of the present and reported deficiencies in the observed data for the Sahel, the shortcomings in the MPAS simulations are in reality most likely smaller.

Regional biases are to a large extent negative. Regarding temperatures, the smallest biases occur in West Africa. The smallest biases in precipitation occur in the eastern part. However, the underestimation in the first case and the overestimation in the second reveal that improvements of the model regarding its physics, land–surface scheme, and land surface input data are required for an adequate simulation of the WA and Sahelian climate.

The results obtained from the two model initialization procedures used are very similar and demonstrate the equivalence of the two approaches. Compared to long term

runs, selections of the initialization years in relation to the spread of mean SST temperatures in the Gulf of Guinea extremely reduce the demand on the CPU, especially when only short terms, such as months or specific seasons, are considered.

Shortcomings in the reproduction of temperatures and precipitation found in the present investigation indicate that the global approach per se does not provide higher fidelity than the regional climate models. Kim et al. (2014) showed that in CORDEX-Africa, multi model ensembles generally outperformed the single ensembles. In such ensemble approaches, MPAS simulations can be applied as an adequate member.

## Open Research

The data generated for this study has been made available at the Radar4KIT repository. The required calculations were performed and figures created by employing the CDO (Schulzweida, 2021), NCO (Zender, 2022), R (R Core Team, 2021) and NCL (NCL, 2021) software packages.

## Acknowledgments

The authors thank the University of Cape Town, South Africa, for providing access to the UCT HPC facility. The study was funded by the German Federal Ministry of Science and Education (BMBF) within the West African Science Service Centre on Climate Change and Adapted Land Use (WASCAL), whose support is gratefully acknowledged.

West African Science Service Centre on Climate Change and Adapted Land Use

## References

- Adeniyi, M., & Oyekola, S. (2017). Assessment of heat and cold wave events over West Africa using three regional climate models. *Ann. Geophys.*, *60*, A0322. doi: 10.4401/ag-7039
- Ahmed, K., Wang, G., Yu, M., Koo, J., & You, L. (2015). Potential impact of climate change on cereal crop yield in West Africa. *Climatic Change*, *133*, 321–334. doi: 10.1007/s10584-015-1462-7
- Arnault, J., Fersch, B., Rummeler, T., Zhang, Z., Quenum, G. M., Wei, J., . . . Kunstmann, H. (2021). Lateral terrestrial water flow contribution to summer precipitation at continental scale – A comparison between Europe and West

- 372 Africa with WRF-Hydro-tag ensembles. *Hydrological Processes*, 35, e14183.  
 373 doi: 10.1002/hyp.14183
- 374 Arnault, J., Knoche, R., Wei, J., & Kunstmann, H. (2016). Evaporation tagging  
 375 and atmospheric water budget analysis with WRF: A regional precipitation  
 376 recycling study for West Africa. *Water Resources Research*, 52(3), 1544–1567.  
 377 doi: 10.1002/2015WR017704
- 378 Broxton, P. D., Zeng, X., Sulla-Menashe, D., & Troch, P. A. (2014). A MODIS-  
 379 Based Global 1-km Maximum Green Vegetation Fraction Dataset. *Journal of*  
 380 *Applied Meteorology and Climatology*, 53, 1593–1605. doi: 10.1175/JAMC-D  
 381 -13-0270.1
- 382 Careto, J. A. M., Cardoso, R. M., Soares, P. M. M., & Trigo, R. M. (2018). Land-  
 383 Atmosphere Coupling in CORDEX-Africa: Hindcast Regional Climate Simula-  
 384 tions. *Journal of Geophysical Research: Atmospheres*, 123(19), 11,048–11,067.  
 385 doi: 10.1029/2018JD028378
- 386 Chen, F., Mitchell, K., Schaake, J., Xue, Y., Pan, H., Koren, V., ... Betts, A.  
 387 (1996). Modeling of land-surface evaporation by four schemes and compari-  
 388 son with FIFE observations. *Journal of Geophysical Research*, 101, 7251–7268.  
 389 doi: 10.1029/95JD02165
- 390 Clough, S., Shephard, M., Mlawer, E., Delamere, J., Iacono, M., Cady-Pereira, K.,  
 391 ... Brown, P. (2005). Atmospheric radiative transfer modeling: a summary of  
 392 the AER codes. *Journal of Quantitative Spectroscopy and Radiative Transfer*,  
 393 91(2), 233-244. doi: 10.1016/j.jqsrt.2004.05.058
- 394 Cook, K. H. (2008). The mysteries of Sahel droughts. *Nature Geoscience*, 1(10),  
 395 647–648. doi: 10.1038/ngeo320
- 396 Coumou, D., & Rahmstorf, S. (2012). A decade of weather extremes. *Nature*  
 397 *Climate Change*, 2, 491–496. Retrieved from [https://doi.org/10.1038/](https://doi.org/10.1038/nclimate1452)  
 398 [nclimate1452](https://doi.org/10.1038/nclimate1452) doi: 10.1038/nclimate1452
- 399 Danielson, J. J., & Gesch, D. B. (2011). *Global multi-resolution terrain elevation*  
 400 *data 2010 (GMTED2010)* (USGS Numbered Series No. 2011-1073). Earth Re-  
 401 sources Observation and Science (EROS) Center. doi: 10.3133/ofr20111073
- 402 Dee, D. P., Uppala, S. M., Simmons, A. J., Berrisford, P., Poli, P., Kobayashi, S., ...  
 403 Vitart, F. (2011). The ERA-Interim reanalysis: configuration and performance  
 404 of the data assimilation system. *Quarterly Journal of the Royal Meteorological*

- 405 *Society*, 137(656), 553–597. doi: 10.1002/qj.828
- 406 Diallo, F. B., Hourdin, F., Rio, C., Traore, A.-K., Mellul, L., Guichard, F., &  
 407 Kergoat, L. (2017). The Surface Energy Budget Computed at the Grid-  
 408 Scale of a Climate Model Challenged by Station Data in West Africa.  
 409 *Journal of Advances in Modeling Earth Systems*, 9(7), 2710–2738. doi:  
 410 10.1002/2017MS001081
- 411 Dieng, D., Smiatek, G., Bliefernicht, J., Heinzeller, D., Sarr, A., Gaye, A. T., &  
 412 Kunstmann, H. (2017). Evaluation of the COSMO-CLM high-resolution  
 413 climate simulations over West Africa. *Journal of Geophysical Research: Atmo-*  
 414 *spheres*, 122, 1437–1455. doi: 10.1002/2016JD025457
- 415 Dilley, M., & Heyman, B. N. (1995). ENSO and Disaster: Droughts, Floods and El  
 416 Niño/Southern Oscillation Warm Events. *Disasters*, 19(3), 181–193. doi: 10  
 417 .1111/j.1467-7717.1995.tb00338.x
- 418 Dosio, A. (2016). Projections of climate change indices of temperature and precip-  
 419 itation from an ensemble of bias-adjusted high-resolution EURO-CORDEX  
 420 regional climate models. *Journal of Geophysical Research: Atmospheres*, 121,  
 421 5488–5511. doi: 10.1002/2015JD024411
- 422 Dosio, A. (2017). Projection of temperature and heat waves for Africa with an en-  
 423 semble of CORDEX Regional Climate Models. *Climate Dynamics*, 49, 493—  
 424 519. doi: s00382-016-3355-5
- 425 Dosio, A., Jury, M., Almazroui, M., Ashfaq, M., Diallo, I., Engelbrecht, F. A., ...  
 426 Tamoffo, A. T. (2021a). Projected future daily characteristics of African  
 427 precipitation based on global (CMIP5, CMIP6) and regional (CORDEX,  
 428 CORDEX-CORE) climate models. *Climate Dynamics*, 57, 3135—3158. doi:  
 429 10.1007/s00382-021-05859-w
- 430 Dosio, A., Lennard, C., & Spinoni, J. (2022). Projections of indices of daily  
 431 temperature and precipitation based on bias-adjusted CORDEX-Africa  
 432 regional climate model simulations. *Climatic Change*, 170(1), 13. doi:  
 433 10.1007/s10584-022-03307-0
- 434 Dosio, A., Panitz, H.-J., Schubert-Frisius, M., & Lühi, D. (2015). Dynamical  
 435 downscaling of CMIP5 global circulation models over CORDEX-Africa with  
 436 COSMO-CLM: evaluation over the present climate and analysis of the added  
 437 value. *Climate Dynamics*, 44(9), 2637–2661. doi: 10.1007/s00382-014-2262-x

- 438 Dosio, A., Pinto, I., Lennard, C., Sylla, M. B., Jack, C., & Nikulin, G. (2021b).  
439 What Can We Know About Recent Past Precipitation Over Africa? Daily  
440 Characteristics of African Precipitation From a Large Ensemble of Ob-  
441 servational Products for Model Evaluation. *Earth and Space Science*, 8,  
442 e2020EA001466. doi: 10.1029/2020EA001466
- 443 Engdaw, M. M., Ballinger, A. P., Hegerl, G. C., & Steiner, A. K. (2022). Changes  
444 in temperature and heat waves over Africa using observational and reanal-  
445 ysis data sets. *International Journal of Climatology*, 42, 1165–1180. doi:  
446 10.1002/joc.7295
- 447 Funk, C., Peterson, P., Peterson, S., Shukla, S., Davenport, J., F. and Michaelsen,  
448 Knapp, K. R., ... Pedreros, N., D. and Mata (2019). A High-Resolution  
449 1983–2016 Tmax Climate Data Record Based on Infrared Temperatures and  
450 Stations by the Climate Hazard Center. *Journal of Climate*, 32, 5639–5658.
- 451 Gbobiya, E., Sarr, A., Sylla, M. B., Diallo, I., Lennard, C., Dosio, A., ...  
452 Lamptey, B. (2014). Climatology, annual cycle and interannual variability  
453 of precipitation and temperature in CORDEX simulations over West Africa.  
454 *International Journal of Climatology*, 34, 2241–2257. doi: 10.1002/joc.3834
- 455 Gelaro, R., McCarty, W., Suárez, M. J., Todling, R., Molod, A., Takacs, L., ...  
456 Zhao, B. (2017). The Modern-Era Retrospective Analysis for Research and  
457 Applications, Version 2 (MERRA-2). *Journal of Climate*, 30(14), 5419–5454.  
458 doi: 10.1175/JCLI-D-16-0758.1
- 459 Glotfelty, T., Ramírez-Mejía, D., Bowden, J., Ghilardi, A., & West, J. J. (2021).  
460 Limitations of WRF land surface models for simulating land use and land  
461 cover change in Sub-Saharan Africa and development of an improved model  
462 (CLM-AF v. 1.0). *Geoscientific Model Development*, 14(6), 3215–3249. doi:  
463 10.5194/gmd-14-3215-2021
- 464 Grist, J. P., & Nicholson, S. E. (2001). A study of the dynamic factors influencing  
465 the rainfall variability in the West African Sahel. *Journal of Climate*, 14(7),  
466 1337 – 1359. doi: 10.1175/1520-0442(2001)014<1337:ASOTDF>2.0.CO;2
- 467 Haile, M. (2005). Weather patterns, food security and humanitarian response in sub-  
468 Saharan Africa. *Philosophical Transactions of the Royal Society B: Biological*  
469 *Sciences*, 360, 2169–2182. doi: 10.1098/rstb.2005.1746
- 470 Harris, I., Osborn, T. J., Jones, P., & Lister, D. (2020). Version 4 of the CRU TS

- 471 monthly high-resolution gridded multivariate climate dataset. *Scientific Data*,  
 472 7. doi: 10.1038/s41597-020-0453-3
- 473 Heinzeller, D., Dieng, D., Smiatek, G., Olusegun, C., Klein, C., Hamann, I., ...  
 474 Kunstmann, H. (2018). The WASCAL high-resolution regional climate simu-  
 475 lation ensemble for West Africa: concept, dissemination and assessment. *Earth*  
 476 *System Science Data*, 10(2), 815–835. doi: 10.5194/essd-10-815-2018
- 477 Heinzeller, D., Duda, M. G., & Kunstmann, H. (2016). Towards convection-  
 478 resolving, global atmospheric simulations with the Model for Prediction Across  
 479 Scales (MPAS) v3.1: an extreme scaling experiment. *Geoscientific Model*  
 480 *Development*, 9, 77–110. doi: 10.5194/gmd-9-77-2016
- 481 Hernández-Díaz, L., Laprise, R., Sushama, L., Martynov, A., Winger, K., & Dugas,  
 482 B. (2013). Climate simulation over CORDEX Africa domain using the fifth-  
 483 generation Canadian Regional Climate Model (CRCM5). *Climate Dynamics*,  
 484 40(5), 1415–1433. doi: 10.1007/s00382-012-1387-z
- 485 Hersbach, H., Bell, B., Berrisford, P., Hirahara, S., Horányi, A., Muñoz-Sabater,  
 486 J., ... Thépaut, J.-N. (2020). The ERA5 global reanalysis. *Quar-*  
 487 *terly Journal of the Royal Meteorological Society*, 146, 1999–2049. doi:  
 488 doi.org/10.1002/qj.3803
- 489 Janicot, S., Moron, V., & Fontaine, B. (1996). Sahel droughts and ENSO dynamics.  
 490 *Geophysical Research Letters*, 23(5), 515–518. doi: 10.1029/96GL00246
- 491 Kanamitsu, M., Ebisuzaki, W., Woollen, J., Yang, S.-K., Hnilo, J. J., Fiorino,  
 492 M., & Potter, G. L. (2002). NCEP–DOE AMIP-II Reanalysis (R-2).  
 493 *Bulletin of the American Meteorological Society*, 83, 1631 – 1644. doi:  
 494 10.1175/BAMS-83-11-1631
- 495 Karl, T., Nicholls, N., & Ghazi, A. (1999). CLIVAR/GCOS/WMO Workshop on  
 496 Indices and Indicators for Climate Extremes Workshop Summary. In T. Karl,  
 497 N. Nicholls, & A. Ghazi (Eds.), *Weather and Climate Extremes* (pp. 3–7).  
 498 Springer, Dordrecht. doi: 10.1007/978-94-015-9265-9\_2
- 499 Kim, J., Waliser, D. E., Mattmann, C. A., Goodale, C. E., Hart, A. F., Zimdars,  
 500 P. A., ... Favre, A. (2014). Evaluation of the CORDEX-Africa multi-RCM  
 501 hindcast: systematic model errors. *Climate Dynamics*, 42(5), 1189–1202. doi:  
 502 10.1007/s00382-013-1751-7
- 503 Klemp, J. B. (2011). A terrain-following coordinate with smoothed coordinate sur-

- 504 faces. *Mon. Wea. Rev.*, *139*, 2163 — 2169. doi: 10.1175/MWR-D-10-05046.1
- 505 Kobayashi, C., & Iwasaki, T. (2016). Brewer-Dobson circulation diagnosed from  
506 JRA-55. *Journal of Geophysical Research: Atmospheres*, *121*, 1493–1510,.  
507 doi: 10.1002/2015JD023476
- 508 Lobell, D. B., Schlenker, W., & Costa-Roberts, J. (2011). Climate trends and global  
509 crop production since 1980. *Science*, *333*(6042), 616–620. doi: 10.1126/science  
510 .1204531
- 511 Maoyi, M. L., & Abiodun, B. J. (2021). How well does MPAS-atmosphere simulate  
512 the characteristics of the Botswana High? *Climate Dynamics*, *57*, 2109–2128.  
513 doi: 10.1007/s00382-021-05797-7
- 514 Masunaga, H., Schröder, M., Furuzawa, F. A., Kummerow, C., Rustemeier, E., &  
515 Schneider, U. (2019). Inter-product biases in global precipitation extremes.  
516 *Environmental Research Letters*, *14*(12), 125016. Retrieved from [https://](https://doi.org/10.1088/1748-9326/ab5da9)  
517 [doi.org/10.1088/1748-9326/ab5da9](https://doi.org/10.1088/1748-9326/ab5da9) doi: 10.1088/1748-9326/ab5da9
- 518 NCL. (2021). *The NCAR Command Language (version 6.6.2) [software]*. Boulder,  
519 Colorado: UCAR/NCAR/CISL/TDD. doi: 10.5065/D6WD3XH5
- 520 New, M., Hewitson, B., Stephenson, D. B., Tsiga, A., Kruger, A., Manhique, A., ...  
521 Lajoie, R. (2006). Evidence of trends in daily climate extremes over southern  
522 and west Africa. *Journal of Geophysical Research: Atmospheres*, *111*(D14).  
523 doi: 10.1029/2005JD006289
- 524 Nicholson, S. E., & Webster, P. J. (2007). A physical basis for the interannual vari-  
525 ability of rainfall in the Sahel. *Quarterly Journal of the Royal Meteorological*  
526 *Society*, *133*, 2065–2084. doi: 10.1002/qj.104
- 527 Nikiema, P. M., Sylla, M. B., Ogunjobi, K., Kebe, I., Gibba, P., & Giorgi, F. (2017).  
528 Multi-model CMIP5 and CORDEX simulations of historical summer tempera-  
529 ture and precipitation variabilities over West Africa. *International Journal of*  
530 *Climatology*, *37*(5), 2438–2450. doi: 10.1002/joc.4856
- 531 Omotosho, J. B., & Abiodun, B. J. (2007). A numerical study of moisture build-up  
532 and rainfall over west africa. *Meteorological Applications*, *14*, 209–225. doi: doi  
533 .org/10.1002/met.11
- 534 Oueslati, B., Pohl, B., Moron, V., Rome, S., & Janicot, S. (2017). Characterization  
535 of heat waves in the Sahel and associated physical mechanisms. *Journal of Cli-*  
536 *mate*, *30*, 3095 – 3115. doi: 10.1175/JCLI-D-16-0432.1

- 537 Panitz, H.-J., Dosio, A., Büchner, M., Lüthi, D., & Keuler, K. (2014). COSMO-  
538 CLM (CCLM) climate simulations over CORDEX- Africa domain: analysis  
539 of the ERA-Interim driven simulations at 0.44 °and 0.22 °resolution. *Climate*  
540 *Dynamics*, 42, 3015–3038. doi: 10.1007/s00382-013-1834-5
- 541 Perkins, D. M., Bailey, R. A., Dossena, M., Gamfeldt, L., Reiss, J., Trimmer, M.,  
542 & Woodward, G. (2015). Higher biodiversity is required to sustain multi-  
543 ple ecosystem processes across temperature regimes. *Global Change Biology*,  
544 21(1), 396–406. doi: 10.1111/gcb.12688
- 545 Poan, E. D., Gachon, P., Dueymes, G., Diaconescu, E., Laprise, R., & Seidou Sanda,  
546 I. (2016). West african monsoon intraseasonal activity and its daily precipi-  
547 tation indices in regional climate models: diagnostics and challenges. *Climate*  
548 *Dynamics*, 47(9), 3113–3140. doi: 10.1007/s00382-016-3016-8
- 549 R Core Team. (2021). *R: A Language and Environment for Statistical Computing*.  
550 <https://www.R-project.org/>.
- 551 Ringard, J., Dieppois, B., Rome, S., Diedhiou, A., Pellarin, T., Konaré, A., ... De-  
552 scroix, L. (2016). The intensification of thermal extremes in west Africa.  
553 *Global and Planetary Change*, 139, 66–77. doi: 10.1016/j.gloplacha.2015.12  
554 .009
- 555 Ringler, T., Thuburn, J., Klemp, J., & Skamarock, W. (2010). A unified ap-  
556 proach to energy conservation and potential vorticity dynamics for arbitrarily-  
557 structured C-grids. *Journal of Computational Physics*, 229, 3065 – 3090. doi:  
558 10.1016/j.jcp.2009.12.007
- 559 Russo, S., Marchese, A. F., Sillmann, J., & Immé, G. (2016). When will unusual  
560 heat waves become normal in a warming Africa? *Environmental Research Let-*  
561 *ters*, 11, 054016. doi: 10.1088/1748-9326/11/5/054016
- 562 Saha, S., Moorthi, S., Wu, X., Wang, J., Nadiga, S., Tripp, P., ... Becker, E. (2014).  
563 The NCEP Climate Forecast System Version 2. *Journal of Climate*, 27, 2185–  
564 2208. doi: 10.1175/JCLI-D-12-00823.1
- 565 Schulzweida, U. (2021). *CDO User Guide (Version 2.0.0)*. doi: 10.5281/zenodo  
566 .5614769
- 567 Sivakumar, M., Collins, C., Jay, A., & Hansen, J. (2014). *Regional priorities for*  
568 *strengthening climate services for farmers in Africa and South Asia* (CCAFS  
569 Working Paper no. 71). Copenhagen, Denmark: CGIAR Research Program on

- Climate Change, Agriculture and Food Security (CCAFS).
- Skamarock, W. C., Klemp, J. B., Duda, M. G., Fowler, L. D., Park, S., & Ringler, D. T. (2012). A Multiscale Nonhydrostatic Atmospheric Model Using Centroidal Voronoi Tessellations and C-Grid Staggering. *Mon. Wea. Rev.*, *140*, 3090 — 3105.
- Smiatek, G., & Kunstmann, H. (2023). Potential impact of the pan-African Great Green Wall on Sahelian summer precipitation: A global modeling approach with MPAS. *Earth Interactions (in Review)*.
- Son, J.-H., & Seo, K.-H. (2020). Mechanisms for the Climatological Characteristics and Interannual Variations of the Guinea Coast Precipitation: Early Summer West African Monsoon. *Atmosphere*, *11*(4). doi: 10.3390/atmos11040396
- Sultan, B., Roudier, P., Quirion, P., Alhassane, A., Muller, B., Dingkuhn, M., . . . Baron, C. (2013). Assessing climate change impacts on sorghum and millet yields in the Sudanian and Sahelian savannas of West Africa. *Environmental Research Letters*, *8*, 014040. doi: 10.1088/1748-9326/8/1/014040
- Sylla, M. B., Gaye, A. T., Pal, J. S., Jenkins, G. S., & Bi, X. Q. (2009). High-resolution simulations of West African climate using regional climate model (RegCM3) with different lateral boundary conditions. *Theoretical and Applied Climatology*, *98*, 293–314. doi: 10.1007/s00704-009-0110-4
- Thuburn, J., Ringler, T., Skamarock, W., & Klemp, J. (2009). Numerical representation of geostrophic modes on arbitrarily structured C-grids. *Journal of Computational Physics*, *228*, 8321 – 8335. doi: 10.1016/j.jcp.2009.08.006
- Xie, P., Chen, M., Yang, S., Yatagai, A., Hayasaka, T., Fukushima, Y., & Liu, C. (2007). A gauge-based analysis of daily precipitation over East Asia. *Journal of Hydrometeorology*, *8*, 607–626. doi: 10.1175/JHM583.1
- Zender, C. (2022). *NCO User Guide*. Department of Earth System Science, University of California, Irvine.